PERGAMON

Journal of Atmospheric and Solar-Terrestrial Physics 60 (1998) 811–829

Journal of ATMOSPHERIC AND SOLAR-TERRESTRIAL PHYSICS

Time resolved N_2 triplet state vibrational populations and emissions associated with red sprites

J. S. Morrill[a,*], E. J. Bucsela[a,f], V. P. Pasko[b], S. L. Berg[c], M. J. Heavner[e], D. R. Moudry[e], W. M. Benesch[d], E. M. Wescott[e], D. D. Sentman[e]

[a] *E. O. Hulburt Center for Space Research, Naval Research Laboratory, Washington, DC, U.S.A.*
[b] *STAR Laboratory, Stanford University, Stanford, CA, U.S.A.*
[c] *Computational Physics Inc., Fairfax, VA, U.S.A.*
[d] *Institute for Physical Science and Technology, University of Maryland, College Park, MD, U.S.A.*
[e] *Geophysical Institute, University of Alaska Fairbanks, Fairbanks, AL, U.S.A.*
[f] *Raytheon STX, Lanham, MD, U.S.A.*

Received 31 March 1997; accepted 11 February 1998

Abstract

The results of a quasi-electrostatic electron heating model were combined with a time dependent N_2 vibrational level population model to simulate the spectral distributions and absolute intensities observed in red sprites. The results include both N_2 excited state vibrational level populations and time profiles of excited electronic state emission. Due to the long atmospheric paths associated with red sprite observations, atmospheric attenuation has a strong impact on the observed spectrum. We present model results showing the effect of atmospheric attenuation as a function of wavelength for various conditions relevant to sprite observations. In addition, our model results estimate the variation in the relative intensities of a number of specific N_2 emissions in sprites (1PG, 2PG, and VK) in response to changes in observational geometry. A recent sprite spectrum, measured from the Wyoming Infrared Observatory (WIRO) on Jelm Mountain, during July, 1996, has been analyzed and includes N_2 1PG bands down to $v' = 1$. In addition to N_2 1PG, our analysis of this spectrum indicates the presence of spectral features which are attributable to N_2^+ Meinel emission. However, due to the low intensity in the observed spectrum and experimental uncertainties, the presence of the $N_2^+(A^2\Pi_u)$ should be considered preliminary. The importance of both the populations of the lower levels of the $N_2(B^3\Pi_g)$ and the $N_2(B^3\Pi_g)/N_2^+(A^2\Pi_g)$ population ratio in the diagnosis of the electron energies present in red sprites is discussed. While the current spectral analysis yields a vibrational distribution of the $N_2(B^3\Pi_g)$ which requires an average electron energy of only 1–2 eV, model results do indicate that the populations of the lower levels of the $N_2(B^3\Pi_g)$ will increase with increases in the electron energy primarily due to cascade. Considering the importance of the populations of the lower vibrational levels, we are beginning to analyze additional sprite spectra, measured at higher resolution, which contain further information on the population of $B(v = 1)$.

1. Introduction

Red sprites are recently-discovered luminous glows occurring above large thunderstorm systems at altitudes typically ranging from 30–90 km. The lateral extent of sprites is typically 5–10 km and they endure for several milliseconds (e.g., Sentman et al., 1995; Funkunishi et al. 1996). Hampton et al. (1996) obtained optical spectra of sprites from the Mt. Evans Observatory on 22 June 1995. The spectra of sprites were also acquired on 16 July 1996 from an observation site near Ft Collins, Colorado, by Mende et al. (1995). The optical spectra were measured in the wavelength range from ~4500–~8400 Å, and four distinct features in the 6000–7800 Å region have been identified as the N_2 First Positive System (1PG, $B^3\Pi_g \rightarrow A^3\Sigma_u^+$) $\Delta v = 2$, 3 and 4 band sequences which reflect emission from vibrational levels 2 through ~8 of the $B^3\Pi_g$. Although the observed emissions were found to be primarily those of the 1PG of N_2, there were also

* Corresponding author. E-mail: morrill@cronus.nrl.navy.mil

S0017-9310/98/$—See front matter
PII: 1364-6826(98)00031-5

indications of the N_2^- Meinel emission ($A^2\Pi_u \rightarrow X^2\Sigma_g^+$) as discussed by Green et al. (1996). More recently, spectroscopic measurements have been made from the Wyoming Infrared Observatory (WIRO) on Jelm Mountain (altitude ~3 km) (Heavner et al., 1996; Bucsela et al., 1998) which extend to longer wavelengths (~9000 Å). These recent measurements include the $\Delta v = 1$ sequence of the N_2 1PG which feature band emissions from the $B^3\Pi_g$ vibrational levels, $v = 1$, 2 and 3.

Spectrally resolved emissions obtained by Mende et al. (1995) and Hampton et al. (1996) have been analyzed in detail by Green et al. (1996) who used energy-dependent electron excitation cross sections and laboratory data to extract information on the energies of electrons producing the sprite radiance. A similar analysis has been performed by Milikh et al. (1997). The results of these steady state models indicate excitation by electrons with a Boltzmann temperature of 1 eV (range 0.4–2 eV). However, Green et al. (1996) suggest that a Druyvesteyn distribution with a suppressed high energy tail may be more realistic. Green et al. (1996) also suggest the presence of N_2^+ Meinel to be important as an indicator of electron energies in sprites, and they present upper bounds on the relative vibrational populations of the $N_2(B)$ and $N_2^-(A)$. Our analysis of the recent sprite spectrum, mentioned above, also indicates the presence of emission features which appear to be due to N_2^- Meinel emissions in addition to the N_2 1PG. However, due to the low intensity the presence of the $N_2^+(A^2\Pi_u)$ and the relative populations of the $N_2^+(A^2\Pi_u)$ and $N_2(B^3\Pi_g)$ states should be considered as being preliminary. Nonetheless, certain spectral features in the observed spectrum are best explained as N_2^- Meinel emissions and, if confirmed, this may have implications relative to the shape of the electron energy distribution. Additional evidence of N_2^+ emission is presented by Armstrong et al. (1998) who report observations of N_2 PG ($C^3\Pi_u$—$B^3\Pi_g$) and N_2^- 1NG ($B^2\Sigma_u^+$-$X^2\Sigma_g^+$). However, unlike the N_2^+ (B) state, $N_2^+(A)$ is reported to be strongly quenched (Vallance Jones, 1974; Piper et al., 1989), and this will be discussed below.

A detailed review of the current theories of sprite production is presented by Rowland (1998). However, we will present here a brief discussion of the three primary theories. The basic mechanism in the quasi-electrostatic model involves the buildup of positive charge in a thundercloud prior to the lightning discharge and the induced space charge in the conducting atmosphere above the thundercloud (Pasko, 1996; Pasko et al., 1997a). When the lightning discharge quickly removes the positive charge, a large quasi-electrostatic field appears at all altitudes above the thundercloud. The resulting field accelerates the ambient electrons and collisionally excites the neutral atmosphere. A similar mechanism to the quasi-electrostatic model is the EMP-induced breakdown which includes the addition of an upward propagating electromagnetic pulse (EMP) associated with a large lightning stroke (Rowland et al. 1996a, b, 1998; Milikh et al. 1995) which can produce breakdown at altitudes above 60 km. The third mechanism involves the possible role of runaway electrons which has been considered by a number of groups (McCarthy and Parks, 1992; Gurevich et al., 1992, 1994; and Roussel-Dupre et al., 1994) who showed that, under certain conditions, secondary cosmic ray electrons with energies of ~1 MeV can become runaway electrons. Model results (Bell et al., 1995) suggest that runaway electrons produce optical emissions similar to the observed spectra when positive cloud-to-ground discharges involve 250 C or more. The threshold runaway field is ~10 times lower than the threshold field of the conventional breakdown and, on this basis, it was suggested by Taranenko and Roussel-Dupre (1996) that the runaway mechanism could proceed at lower quasi-electrostatic field levels.

It is now well known (Sentman et al., 1996; Wescott et al., 1996; Taylor and Clark, 1996) that, rather than simply diffuse and unstructured, sprites are in fact highly structured and that they continue to produce significant emission for relatively long periods (some tens of ms) and show 'rebrightening'. Indeed, under certain geophysical conditions the electric breakdown associated with sprites may develop in the form of streamers (Stanley et al., 1996; Fukunishi et al., 1996). The electric field in very narrow regions around the tips of streamers (scale ~1 m at 70 km altitude) can be much greater than the breakdown field and generally lead to localized enhancements in N_2 2PG and N_2^+ 1NG emissions in comparison with N_2 1PG emissions (Pasko et al., 1997b). Within most of the volume of the sprite and during a majority of the time associated with the sprite, the electric field is expected to remain at the level only slightly above the breakdown field. From simple physical arguments, it is clear that new ionization produced by the discharge would tend to reduce the electric field due to the enhancement in conductivity. However, rather than examine the detailed spatial structure observed in sprites, in this paper we consider the spectrum summed over several scan lines to improve the signal to noise ratio.

Specifically, in this paper we use a quasi-electrostatic (QE) model of lower ionospheric/mesospheric heating and ionization (Pasko et al., 1997a), a recently developed time dependent model of N_2 triplet state vibrational populations (Morrill and Benesch, 1990; 1996), and an atmospheric transmittance model, MOSART (Cornette et al., 1994), to perform detailed time dependent simulations of the N_2 emissions associated with sprites. Model $N_2(B)$ vibrational distributions, summed over ~30 ms, agree reasonably well with those resulting from fitting the spectral observations of Mende et al. (1995) and Hampton et al. (1996) to the 1PG system of N_2 (Green et al., 1996). The current results also provide predictions for future spectral or photometric observations ranging

from UV (Vegard-Kaplan (VK), Second Positive (2PG)) through the visible to the near-infrared (1PG), and the variety of observational geometries, including observations from the ground, mountains, aircraft and balloons. We analyze one of the recent spectra measured from Jelm Mountain, WY, in July 1996 (Heavner et al., 1996; Bucsela et al., 1998) and the resulting vibrational distributions of the $N_2(B)$ and $N_2^+(A)$ states are presented below along with the recent populations determined by Green et al. (1996). As is the case in the aurora (Cartwright, 1978), it is found that the relative populations of the lower $B^3\Pi_g$ levels are important indicators of the electron energies in red sprites. In addition, the possible presence of the $N_2^+(A)$ Meinel emission has implications regarding the electron energy distribution (Green et al., 1996). The current $N_2(B)$ vibrational distribution, as with Green et al. (1996), indicates a low electron energy ($\sim$1–2 eV). However, the possible presence of the $N_2^+(A)$ Meinel emission implies a much higher average electron energy ($> \sim 10$ eV) or an enhancement in the high energy tail of the electron energy distribution.

2. Atmospheric transmission

Spectroscopic studies of sprites generally entail observations made across long, nearly horizontal paths through the atmosphere. Observations of the aurora, in contrast, are seldom affected by path lengths more than a few percent longer than a single vertical path through the atmosphere. Accordingly, while auroral spectra in the visible and near ultraviolet are only minimally distorted by atmospheric absorption and scattering, these processes constitute major factors in the production of the apparent spectrum of a sprite as observed from platforms at different altitudes (e.g., ground, aircraft, or balloons). This distortion must be accounted for in order to determine the vibrational distributions associated with an observed spectrum (Green et al., 1996).

It is molecular absorption and scattering that primarily contribute to the attenuation of the spectra of sprites. Ozone, oxygen and water vapor are the main absorbers through the visible and near infrared, while Rayleigh scattering dominates the shorter wavelengths. The influences of these mechanisms have been taken into account in the present model. Their impact on the sprite spectrum as calculated for various paths through the atmosphere is displayed by Fig. 1.

The atmospheric transmission profiles in Fig. 1 were calculated by the Moderate Spectral Atmospheric Radiance and Transfer (MOSART) model (Cornette et al., 1994) as implemented in the Naval Research Laboratory's Synthetic Scene Generation Model (SSGM) (Wilcoxen and Heckathorn, 1996). This model was used to generate atmospheric transmittance with a spectral resolution of 5 cm^{-1} between an emission point at 65 km and an observation point at a lower altitude (0–20 km). MOSART is local thermodynamic equilibrium (LTE) model and has combined the best features of the Air Force Phillips Laboratory's MODTRAN code (Berk et al., 1989) and the Atmospheric Propagation and Radiative Transfer (APART) model (Cornette, 1990). MOSART contains all of the atmospheric features of MODTRAN. The MODTRAN one-dimensional Mid-latitude Summer model atmosphere was used for these calculations.

Figure 1 shows the wavelength dependent transmission of the atmosphere from an altitude of 65 km to the observation altitudes indicated on the figure (0, 5,10, 20 km) along two different path lengths (a) 100 and (b) 500 km. The observation altitudes (0, 5, 10, 20 km) were chosen to be representative of observations from the ground, mountains, aircraft and balloons, respectively. The 20 km altitude would also include high altitude aircraft such as the U2 and WB-57F. The actual path lengths and zenith angles associated with Fig. 1 are presented in Table 1.

As Fig. 1 indicates, the atmosphere permits the transmission of sprite radiation beginning at the long-wavelength end of the absorption by the ultraviolet bands of ozone at about 3000 Å, depending on path length. For the longer path lengths, transmission has already been much attenuated below 4000 Å by Rayleigh scattering. Ozone again contributes significant absorption via the Chappius bands which are broad and diffuse with peaks at about 5730 and 6020 Å. Vibrational bands of water vapor then appear and become increasingly significant into the infrared. The sharp double peak near 7600 Å is due to molecular oxygen, the (0–0) O_2 Atmospheric band, and serves to cut into the $\Delta v = 2$ sequence of the sprites First Positive spectrum of N_2.

3. Spectral analysis

Prior to the determination of the vibrational distribution associated with an observed spectrum, the atmospheric attenuation must be accounted for (Green et al., 1996). This was accomplished by scaling the synthetic 1PG v' progressions (common upper vibrational level) with the model atmospheric transmission and then using a least-squares spectral fitting procedure. Our analysis of the N_2 1PG spectrum measured from Jelm Mountain, during July 1996, mentioned above, extends up to $\sim$9000 Å and was done assuming a 520 km path length, an emission altitude of 57 km and an observation altitude of $\sim$3 km, as determined from the video image taken simultaneously with the spectrum. The superposition of the spectrograph slit on the video image of the sprite shows the spectrum to be of an upper portion of a tendril which extends downward from the main body of the sprite. This 1PG spectrum includes emission of the $\Delta v = 1$

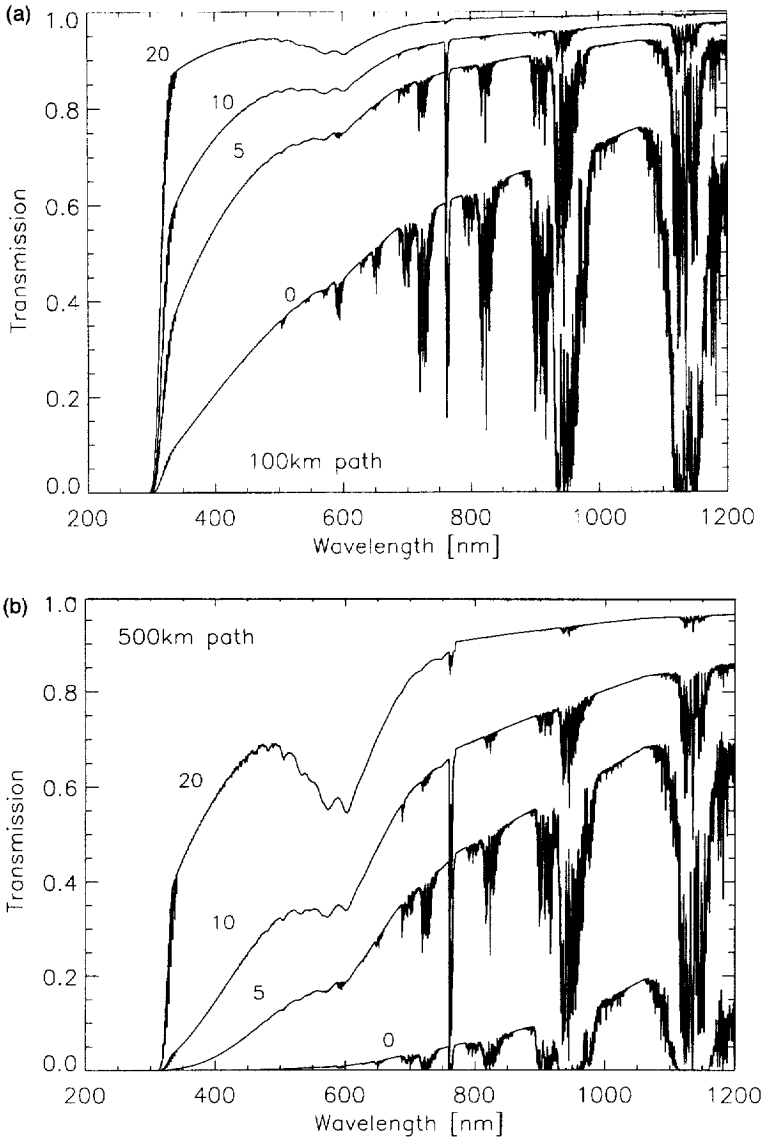

Fig. 1. Atmospheric attenuation between 65 km and observation altitudes of 0, 5, 10 and 20 km along (a) 100 km and (b) 500 km path lengths.

sequence and so provides a measure of the relative population of the $v = 1$ level of the $B^3\Pi_g$ through the intensity of the (1,0) band with a band origin at 8884 Å (Gilmore et al., 1992). We have also included the N_2^+ Meinel transition in our analysis and a number of bands of this system are indicated in the fit of this spectrum. Previous measurements of sprite spectra were done for emission from higher altitudes (Mende et al., 1995; Hampton et al., 1996) and our choice of altitudes for the modelling portion of this study (65 and 75 km) was based on these values. However, a detailed examination of the observational geometry determined the 57 km altitude of emission associated with the sprite spectrum in Fig. 2.

The details of the spectral analysis routine are given elsewhere (Bucsela and Sharp, 1997) but we present a brief description here. A multiple linear regression algorithm was used to determine the relative intensities of the molecular band progressions in the spectrum. The procedure is similar to that employed by Fraser et al., (1988). A set of unit-intensity 1PG vibrational bands are each multiplied by an intensity scaling factor and combined with the other bands to produce a synthetic

Table 1
Atmospheric attenuation: actual path lengths and zenith angles

Observation altitude (km)	Path length (km)		Zenith angle (°)	
	100	500	100	500
0	107.3	495.5	53.1	84.7
5	104.4	495.1	55.3	85.2
10	101.6	494.7	57.6	85.8
20	96.7	494.1	62.6	87.0

The actual path lengths and zenith angles used in the calculation of atmospheric attenuation. The column headings '100' and '500' correspond to the nominal path lengths shown in Fig. 1.

spectrum. The intensities are varied independently to minimize the chi-square in fitting the features to the data. The features included in the fit were the (1, 0) band, the (v'-v'') progressions (2, 0–1), (3, 0–3), (4, 0–4), (5, 0–5), (6, 2–6), (7, 3–8), (8, 4–9) for the N_2 1PG and the (v'-v'') progressions (2, 0–1) and (3, 0–2) for the N_2^+ Meinel, as well as a uniform continuum background. Progressions originating from higher v' levels in both band systems proved too weak to yield meaningful intensities when fitted to the spectrum. Also, negative intensities for several band progressions resulted when the background level was allowed to vary freely in the fit. Therefore the background was fixed at a level just below its fitted value so that all feature intensities were positive.

Shapes of the vibrational bands were calculated by synthesizing the rotational lines of molecular band progressions and multiplying by an atmospheric transmittance profile, as already described. The attenuated features were convolved with a Gaussian function representing the instrumental line shape. The resolution was varied from a full width at half maximum of 9 nm at the shorter wavelengths to 14 nm at 1000 nm and this was found to produce the best fit to the spectral data. The rotational line strengths and wavelengths were calculated with a band synthesis algorithm that has been described by Bucsela and Sharp (1994). Molecular constants for the N_2(A) and N_2(B) states and the N_2^+(X) and N_2^+(A) states were obtained from Laher and Gilmore (1991) and Huber and Herzberg (1979), and the relative intensities of bands within the progressions were fixed according to the transition probabilities of Gilmore et al. (1992). The temperature of all bands was set at 230 K but, due to the current resolution, the fit was relatively insensitive to the choice of rotational temperature.

Figure 2a shows the observed spectrum corrected for instrument sensitivity as well as our best fit which includes both 1PG and Meinel band emissions. In this figure the observed spectrum is shown by the solid line, the full spectral fit (1PG+Meinel) by the dashed line, and the Meinel portion by the dotted line. The resulting N_2 ($B^3\Pi_g$) vibrational distribution appears in Fig. 2b as well as the N_2^+ ($A^2\Pi_u$) populations for levels 2 and 3. The overall scale is arbitrary but the relative population of the N_2 (B) and N_2^+ (A) vibrational levels has been preserved.

The presence of the Meinel band in the 55–60 km altitude region is difficult to explain since this emission has a quenching height of 85–90 km (Vallance Jones, 1974). Consequently, we have attempted to fit the observed spectrum without the Meinel band and we are currently preparing these results for inclusion in a publication discussing the analysis of a number of other sprite spectra (Bucsela et al., 1998). Our attempt to fit this emission without the Meinel band produced two basic scenarios regarding the observed emission in the 7800–8200 Å region. First, if the spectral fitting model is constrained as it is with the Meinel bands present (e.g. the weight associated with the intensity at a specific wavelength is based on the noise in the calibrated spectrum at that wavelength), then the model produces a good fit to the emission at most wavelengths except the region between 7800 and 8200 Å which is very poorly fitted. Furthermore, the observed spectrum appears to have excess emission in this wavelength range. Secondly, if the model is constrained to fit only the longer wavelengths (> 7300 Å), then the 7800 to 8200 Å region is well fitted. However, in this case the model spectrum contains tremendous enhancements near 6550 and 7650 Å, largely due to $v' = 7$ band emissions. These enhancements are beyond anything explainable in terms of uncertainty in the observed spectrum. In addition to the spectral fitting, significant effort has been expended to ensure that all data processing and calibrations have been done properly. Although the possibility remains that the features in the 7800–8200 Å region are due to either an instrumental or processing artifact which has not been considered, we are forced to conclude that the observed spectrum in this region is best explained as Meinel emission. In order to confirm these results, we are currently examining additional sprite spectra to determine if the emission in the 7800–8200 Å appears during other observations.

4. Quasi-electrostatic model

The electric field transients capable of causing breakdown ionization at mesospheric altitudes can be produced by cloud to ground lightning discharges removing large amounts of positive thundercloud charge on a time scale of several milliseconds (Pasko et al., 1995, 1997a). The quasi-electrostatic (QE) heating model quantitatively describes the evolution of the electric field in the conducting atmosphere resulting from a given charge dynamics at tropospheric altitudes (e.g., accumulation of thundercloud charge and its removal by lightning). The electric field and charge density are calculated using the Poisson and continuity equations. The conductivity of

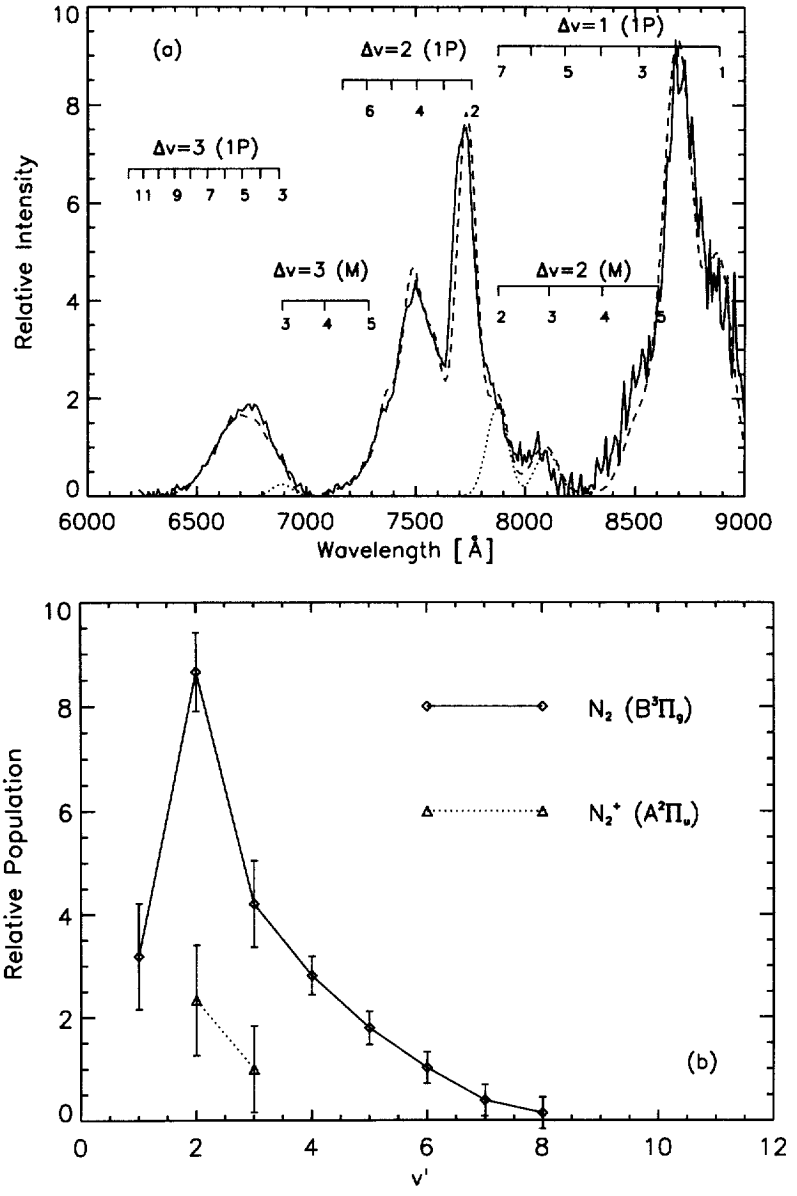

Fig. 2. (a) Sprite spectrum and least-squares fit which consists of the 1PG spectrum of N_2 and the Meinel spectrum of N_2^+: (b) $N_2(B)$ and $N_2^+(A)$ vibrational distributions determined by the fit.

the medium is calculated self consistently by taking into account the effect of the electric field on the electron component through changes in mobility (due to heating) and electron density (due to ionization). A detailed description of the QE model is presented by Pasko (1996) and Pasko et al. (1997a).

It is important to note that results of the QE model generally demonstrate large variability as a function of input parameters (e.g., altitude profile of atmospheric conductivity, discharge duration and thundercloud charge geometry (Pasko et al., 1997a)). This is a direct consequence of the highly nonlinear nature of the interaction of thundercloud electric fields with the mesosphere/lower ionosphere, leading to large heating and ionization changes, which significantly modify the ambient conductivity. In spite of this large variability, under a variety of conditions the magnitude of the electric field does not significantly exceed the characteristic air breakdown field E_k (which varies proportionally to the ambient air density, N (e.g., Papadopoulos et al., 1993)). This

effect is mostly defined by the fast (~ 1 ms) screening of the electric field due to enhancements of the conductivity produced by the breakdown ionization and leads to an important conclusion that spectral results obtained for the limited number of cases considered in this paper are valid for much wider range of input parameters (not only those chosen here for the calculations). It is important to note in this regard that heated electron energy distributions are self similar at different altitudes for the electric fields $E \sim E_k$ (i.e., remain the same for the same E/N ratios).

For the purpose of the studies in this paper we take a case of the removal of 475 Coulombs of charge from altitude 10 km in 20 ms (called case (e) in Pasko et al. (1996)), associated with the formation of a columnar channel of breakdown ionization and relatively long optical emission. This case leads to the intense production of excited electronic states at higher altitudes (>65 km) which makes it preferable in comparison with other similar cases in (Pasko et al., 1996c, d) from the point of view of the application of existing vibrational population models (see next section). The dynamics of the electric field and electron number density are readily calculated by the model at any time during the 100 ms period considered. Figures 3 and 4 show these two quantities as a function of time and at two selected altitudes 65 and 75 km. The characteristic breakdown field E_k at these altitudes is also shown in Fig. 3 by horizontal dashed lines.

The electric field and electron density values shown in Figs 3 and 4 are used to calculate the temporal variation of the electron distribution function $\Phi(\varepsilon)$ in units of (1/cm^2-s-eV) (here ε is the electron energy) using the solution of the Boltzmann equation, taking into account inelastic collisions consisting of rotational, vibrational, optical, dissociative, dissociative with attachment and ionizational losses (Taranenko et al., 1993a, b). Results are shown in Fig. 5a and b for altitudes 65 and 75 km, respectively, at selected instants of time.

The average energy of the electron distribution is shown in Fig. 6, demonstrating that the average energy does not exceed 5.5 eV. This indicates that most of the ionization is produced by the relatively small number of electrons in the tail of the electron distribution function which appear in the region of energies of ~ 15 eV (corresponding to the ionization threshold of N_2 and O_2). Lastly, Fig. 7 shows the temporal variation in the production rate of vibrationally excited N_2 calculated using the electron energy distribution functions and known cross section of this process (Taranenko et al., 1993a, b; Phelps, 1987).

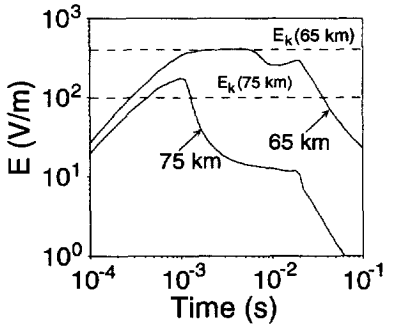

Fig. 3. The electric field as a function of time at two selected altitudes 65 and 75 km. The characteristic breakdown field corresponding to each altitude is shown by horizontal dashed lines.

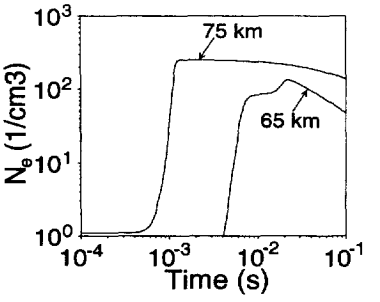

Fig. 4. The electron number density as a function of time at two selected altitudes—65 and 75 km.

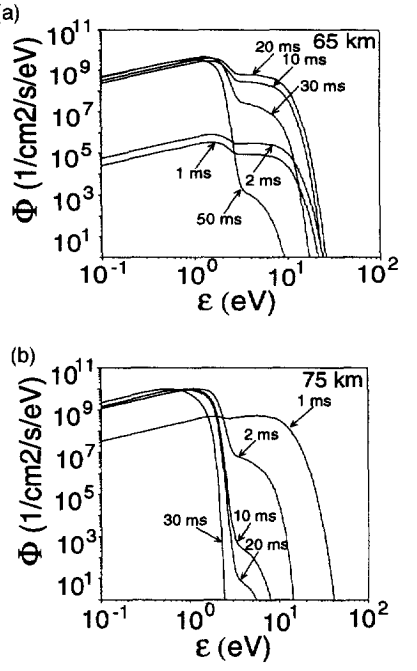

Fig. 5. The distribution of heated electrons as a function of energy at selected instants of time, and at two selected altitudes (a) 65 and (b) 75 km.

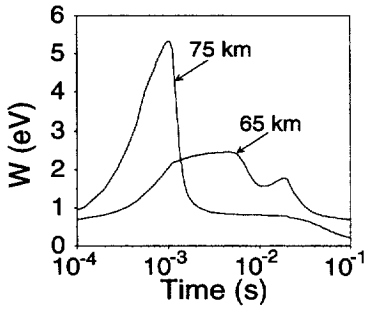

Fig. 6. The temporal variation of the average electron energy at two selected altitudes, 65 and 75 km.

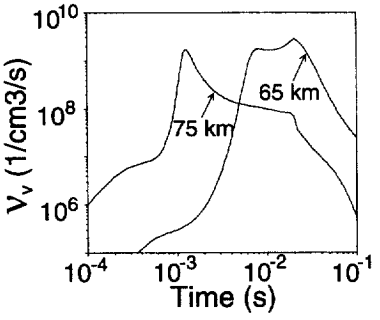

Fig. 7. The production rate of vibrationally excited N_2 as a function of time at two selected altitudes, 65 and 75 km.

5. Vibrational level populations model

In order to examine the details of the time dependent variations of red sprites, we have adapted a number of steady state kinetic models of the vibrational level populations of the N_2 triplet states. These models have been used to examine N_2 emissions in low altitude aurora (Benesch, 1981, 1983; Morrill and Benesch, 1996) and under airglow conditions (Bucsela and Sharp, 1997). They are both variations of the earlier model developed by Cartwright (1978). The time dependent model was originally developed for the analysis of laboratory observations of pulsed laboratory discharges (Carragher et al., 1991a, b; Morrill et al. 1988, 1991; Morrill and Benesch, 1990, 1994) which involved shorter excitation pulses and more complex afterglow processes (such as energy pooling (Piper, 1988, a b, 1989)) than were expected in sprites. The current model has been adapted to work with a longer excitation and decay time and presently covers a 100 ms period. The time resolution for each iteration has been kept short (0.5 μs) but the results have been binned into 20 μs bins. Considering the photometric observations of Fukunishi et al. (1996), we regard this combination of decay period and time resolution to be adequate to model the emissions throughout the duration of a typical red sprite ($\sim$1–10 ms).

Table 2
MSIS densities and temperatures

Parameter	65 km	75 km
N_2 (/cm^3)	3.06e15	7.32e14
O_2 (/cm^3)	8.20e14	1.95e14
O (/cm^3)	0.0	1.4e8
T(K)	227.2	195.8

The MSIS 90 model atmosphere densities and temperatures used in the calculation of the excited electronic state populations.

In addition to electron impact excitation and radiative cascade, the time dependent model also contains the collisional processes utilized in the steady state model discussed by Morrill and Benesch (1996). The three collisional processes are simple quenching, intersystem collisional transfer (ICT) (Benesch, 1981, 1983), and vibrational redistribution within the $A^3\Sigma_u^+$ vibrational manifold. Briefly, quenching involves the complete loss of electronic excitation from the N_2 triplet state manifold and is distinctly different from the collisional transfer of electronic excitation and vibrational redistribution. For these latter two processes, electronic excitation is retained and is either transferred to an adjacent electronic state (e.g. from $B^3\Pi_g$ to $A^3\Sigma_u^+$, $W^3\Delta_u$, or $B'^3\Sigma_u^-$) or retained by the $A^3\Sigma_u^+$ with the loss of some number of vibrational quanta into the ground state vibrational manifold (Morrill and Benesch, 1996). A similar analysis involving collisional transfer among the N_2 singlet states has recently been presented by Eastes and Dentamaro (1996). The model requires density and temperature values from an atmospheric model. Kinetic temperatures and densities for N_2, O_2 and O from the MSIS 90 model atmosphere (Hedin, 1991) were used as inputs and these values appear in Table 2.

Observations indicate that the N_2 1PG is the dominant red emission in sprites (Mende et al., 1995; Hampton et al., 1996) that is produced by emission from the $B^3\Pi_g$. Once the observed band intensities are corrected for atmospheric attenuation, they are a direct measure of the populations of the vibrational levels. In order to model these populations under steady state conditions, the ratio of the production and loss rates are iterated until the model populations come to equilibrium. With the time dependent model, the effect of the production and loss rates on the population of each individual level is calculated for a small time step and then added to or subtracted from the population at the previous time interval. These rates can vary with time due to changes in electron energy, which affects direct electron excitation, or with upper state population, which affects cascade. The variation of the production and loss rates, along with the short lifetime of the $B^3\Pi_g$, has determined the size of time

interval (0.5 μs) in the current calculation. The field observations have used video format with a time resolution of the order of 17–33 ms. Consequently, we examine $B^3\Pi_g$ vibrational distributions summed over a period of 30 ms for comparisons with these observations. This time period includes the majority of the predicted emission at both altitudes modeled in this study (65 and 75 km).

In the current model we have not included the time variation of the ground state vibrational distribution. The ground state distribution determines the initial excited state vibrational distributions produced during electron impact excitation. As has been noted elsewhere (Morrill and Benesch, 1990), variation in the excited vibrational distribution can be significant but only when the vibrational temperature increases from lower temperature (~100–300 K) to values on the order of 1500–2000 K. The temporal variation of the N_2 ground state vibrational distribution is a complex process involving both production by electron impact excitation and loss by interactions with atomic and molecular species in the atmosphere (Caledonia and Center, 1971; Torr and Torr, 1982; Pavlov and Buonsanto, 1996), and we will examine this in a future publication. In the current model the vibrational temperature is chosen to be the kinetic temperature (Table 2) and this is maintained throughout the 100 ms period.

6. Model results and data comparison

The calculation of the time dependent populations uses the electron energy distributions shown in Fig. 5. These distributions were used with the electron impact excitation cross-sections (Trajmar et al. 1983; Zubek, 1994; Zebek and King, 1994) to determine the excitation rates for the seven triplet states used in the current model, $A^3\Sigma_u^+$, $B^3\Pi_g$, $W^3\Delta_u$, $B'^3\Sigma_u^-$, $C^3\Pi_u$, $D^3\Sigma_u^+$, $E^3\Sigma_g^+$ (See Cartwright (1978) or Morrill and Benesch (1996)). The resulting excitation rates are plotted in Fig. 8. These results indicate that excitation continues for much longer at 65 km than at 75 km. Note that at 75 km (Fig. 8b) the excitation is confined to a single spike which is less than ~5 ms wide while our results at 65 km (Fig. 8a) show that the excitation begins later (~5 ms) but continues until ~20–25 ms. Also, there is a plateau in the 75 km excitation rates between 5 and 20 ms (not shown), but the rates have dropped to such small relative values that there is no significant effect on the model populations or predicted intensity during this period. This behavior is a direct result of the faster relaxation of the electric field at higher altitudes (Fig. 3), leading to faster cooling of the electron energy distribution (Fig. 5a).

Using the excitation rates in Fig. 8, we have calculated the time dependent vibrational populations of the seven triplet states presented above (Morrill and Benesch, 1996). Due to differences in the excited state lifetimes and excitation cross sections, it is difficult to illustrate the temporal behavior of the absolute value of the excited state populations predicted by the model. Consequently, we begin with an example comparing the population of $v = 0$ of the A, B, W, B′, and C states, normalized at the peak for 75 km with quenching only (Fig. 9). As expected, this figure shows that the emission from the longer lifetime species peaks later, following the onset of the excitation pulse. Figure 9 shows the decay of both A(0) and W(0) to be dominated by quenching, since both levels have much longer lifetimes than indicated by these curves (τ(A(0)) ~2.4 seconds and τ(W(0)) ~0.17 seconds).

Next, the predicted number density of ($v = 0$) for the above five states in Fig. 9, is shown in Fig. 10 where we now examine the results for 65 km. Figure 10b shows a number of effects when the additional collisional processes are included (QIR), the predicted enhancement in A(0), the equilibration of overlapping populations (B(0) and W(0)), and an enhancement in B′(0) (compare Fig. 10a and 10b). Note that in Fig. 10b, the number density of B(0) and W(0) levels overlap (the second curve from the top) and the levels are said to be collisionally coupled. Similar behavior is predicted for these two levels at 75 km altitude. Also, Fig. 10b shows the predicted enhancement in the B(0) population produced by including collisional transfer (ICT) in addition to simple quenching (Fig. 10a). This enhancement will lead to increases in overall 1PG band intensity (Morrill and Benesch, 1996).

An important point regarding Fig. 10 involves the significant density of A(0). At both altitudes and with either set of collisional processes, the density is predicted to exceed 10^5 mol/cm^3 for ~15–20 ms. The rapid decay of A(0) compared to that expected due to radiative decay indicates the effect of strong quenching, primarily by O_2 (Cartwright, 1978; Morrill and Benesch, 1996). Processes involving N_2(A) energy pooling, where energy transfer occurs from the N_2(A) state to both the N_2(C) and N_2(B) states (Piper, 1988a, b; 1989), are not included in the current analysis but we briefly discuss these processes below.

Summing the B state populations over the first 30 ms gives the vibrational distribution that would be observed by a spectrograph operating at video frame rates. Figure 11 is a comparison of a number of different model vibrational distributions with those determined from the observations discussed above. The distributions from the observations were determined by Green et al. (1996) and our analysis presented earlier. Figure 11a and b compares model distributions at 65 km and 75 km, respectively. All populations are expressed as a percentage of the total populations of level 2 and 4 through 8. The populations of $v = 1$ and 3 are excluded from the normalization of the observed populations due to uncertainties in both the 1PG (3, 0) intensity associated with absorption by the O_2 Atmospheric (0, 0) band at 7594 Å and by the fact that $v = 1$ is determined from a single band, 1PG (1, 0), at the very edge of the red sensitive portion of the spectrum.

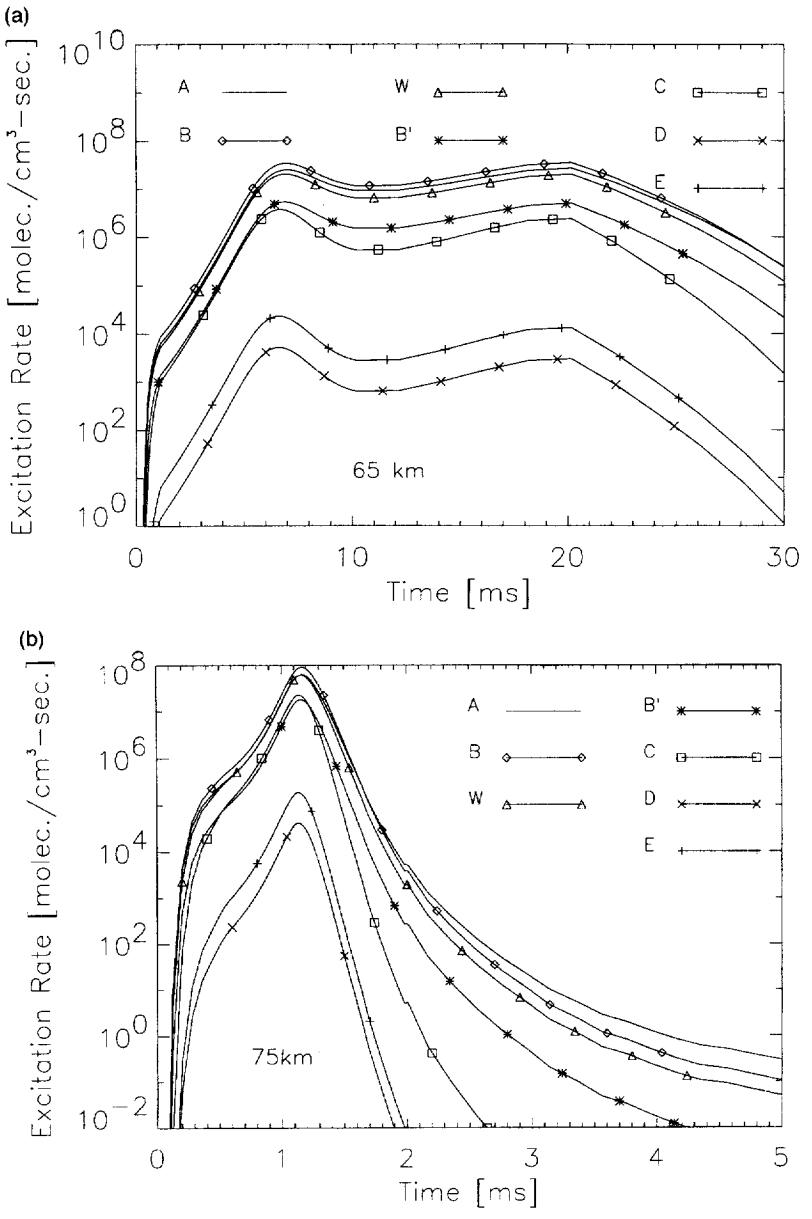

Fig. 8. Excitation rates of seven N_2 triplet states at (a) 65 km and (b) 75 km.

Two different model distributions are shown in Fig. 11 for the case of quenching only (solid line) and for the case where all collisional processes are included (dashed line). It is notable that, although the model distributions generally fit those derived from the observed spectra, neither model result is able to reproduce the enhancement in $v = 2$ or the de-enhancement in the higher levels. Similar difficulties appear to have been encountered by Green et al. (1996; Fig. 3). In addition, the population of $v = 1$ appears low based in comparison with model results as well as laboratory pulsed discharge spectra (Morrill and Benesch, 1988, 1990, 1994). This low value is possibly due to calibration uncertainties since the (1, 0) band occurs at a wavelength where the spectrograph sensitivity is rapidly decreasing (~9000 Å). To estimate the difference between the model and observed $v = 1$ populations, the observed value has been scaled by 1.5 and 2.0, and is also plotted in Fig. 11. Preliminary estimates of the $v = 1$ populations measured at higher resolution and with better red sensitivity (see above) indicate that the $v = 1$ population is on the order of twice the value implied by the lower resolution spectrum shown in Fig. 2a.

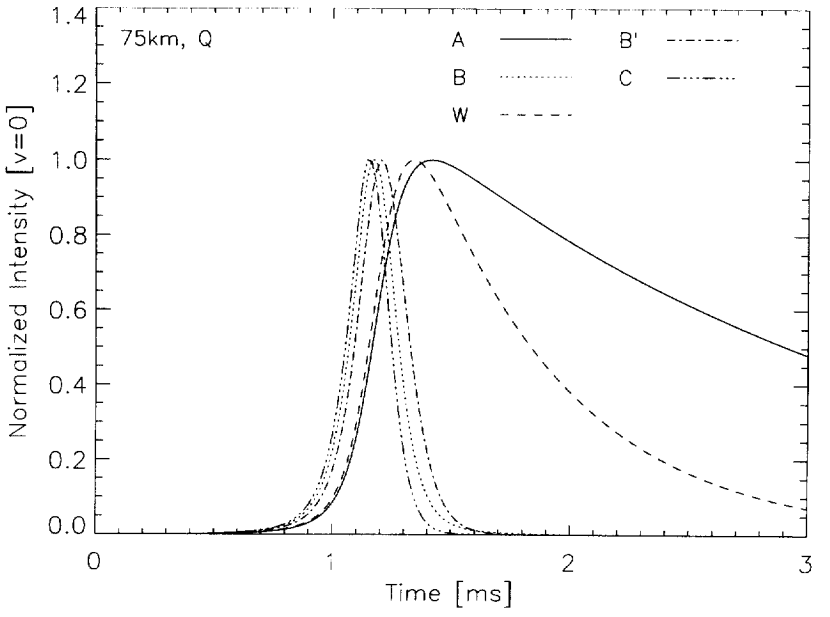

Fig. 9. Normalized triplet populations ($v = 0$) with quenching (Q) only at 75 km.

Also shown in Fig. 11 is the model vibrational distribution characteristic of an aurora at 110 km (Morrill and Benesch, 1996; Fig. 8). The most obvious difference between the auroral distribution and those observed or modeled in sprites is the enhancement of the populations of the lower $N_2(B)$ vibrational levels in the auroral case. The auroral distribution reflects excitation by a higher energy distribution of electrons than that expected in sprites. In fact, the enhancement in the lower vibrational level populations under auroral conditions is due largely to increases in cascade from the $N_2(C)$ via the 2PG ($C^3\Pi_u \rightarrow B^3\Pi_g$) (Cartwright, 1978). The effect of increasing the electron energy distribution can be seen by comparing the model vibrational distributions in Fig. 11, where the average energy has a larger peak value at 75 km (Fig. 11a) than at 65 km (Fig. 11a), as shown in Fig. 6. In addition, the observed auroral $N_2(B)$ vibrational distributions (Vallance Jones and Gattinger, 1976, 1978) show an enhancement in $v = 2$ not completely explained by the model (Morrill and Benesch, 1996; Fig. 8), similar to the enhancement in the sprite distribution. Similar strong enhancements in $v = 2$ have also been observed in the laboratory between 30 and 1000 mTorr in radio frequency discharge and during the afterglow (either following a pulsed discharge or in a flow reactor).

These enhancements in the $B(v = 2)$ population are produced by a number of processes. In a laboratory discharge at constant pressure, the enhancements are due to a combination of quenching and energy transfer (ICT) as well as energy pooling reactions (Benesch and Fraedrich, 1984; Morrill 1986). In the afterglow the enhancements are primarily due to energy pooling processes involving reactions of the $N_2(A)$ state with other $N_2(A)$ molecules or with vibrationally excited ground state molecules (Piper, 1988a, b; 1989). The apparent enhancement in the aurora at 110 km (Vallance Jones and Gattinger, 1976; 1978) is more difficult to explain and may imply a larger ICT or smaller quenching rate coefficient associated with $v = 2$ than are currently used in the steady state model (Morrill and Benesch, 1996).

Finally, in an effort to estimate the effect of errors associated with the rate coefficients, a single model run at 65 km was performed with all of the collisional rate coefficients increased by 20%. This resulted in an approximately 6% reduction in the overall population of the $N_2(B)$ state, indicating that the model populations are relatively insensitive to small errors in the rate coefficients. However, at 65 km and below, where collisions are much more frequent than at 75–100 km, the effect of errors $>20\%$ in the collisional rate coefficients will have a larger impact on the final distributions predicted for the lower altitudes. In an effort to improve the fit between the model and observed vibrational distributions, we are currently reexamining both the quenching and collisional transfer rate coefficients used in our kinetic model.

7. Discussion

The nature of sprite observations involves long atmospheric path lengths which result in significant attenu-

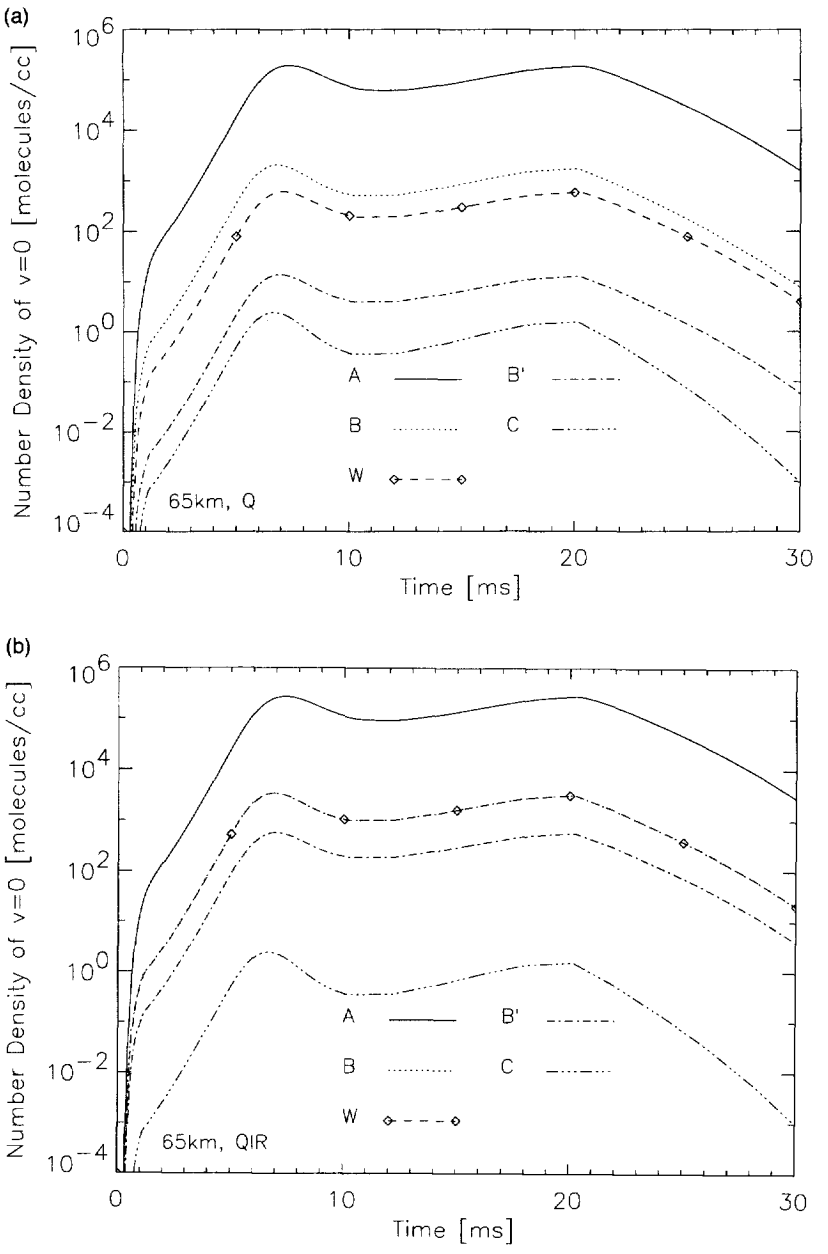

Fig. 10. Predicted number density of $v = 0$ for (a) quenching only (Q) and (b) quenching, ICT, vibrational redistribution (QIR) at 65 km.

ation of the emitted spectrum. This leads to uncertainties in the vibrational distribution determined by the spectral fit and estimates of absolute intensities. Such information is important in determining of the role of initial electron excitation and subsequent energy transfer and relaxation processes. The accurate evaluation of these processes will be aided by improvements in both kinetic rate coefficients and data quality. Improvements in rate coefficients may require further laboratory studies. Improvement in data are expected as improvements in instrumentation and observing conditions are implemented. However, given the faint and elusive nature of the observed phenomenon, this is a demanding requirement. As shown in Fig. 1, by reducing the path length between the sprites and the observer as well as increasing the altitude of the observation point, substantial improvement in data quality can be achieved without any changes in instrumentation. This improvement is especially evident for emissions

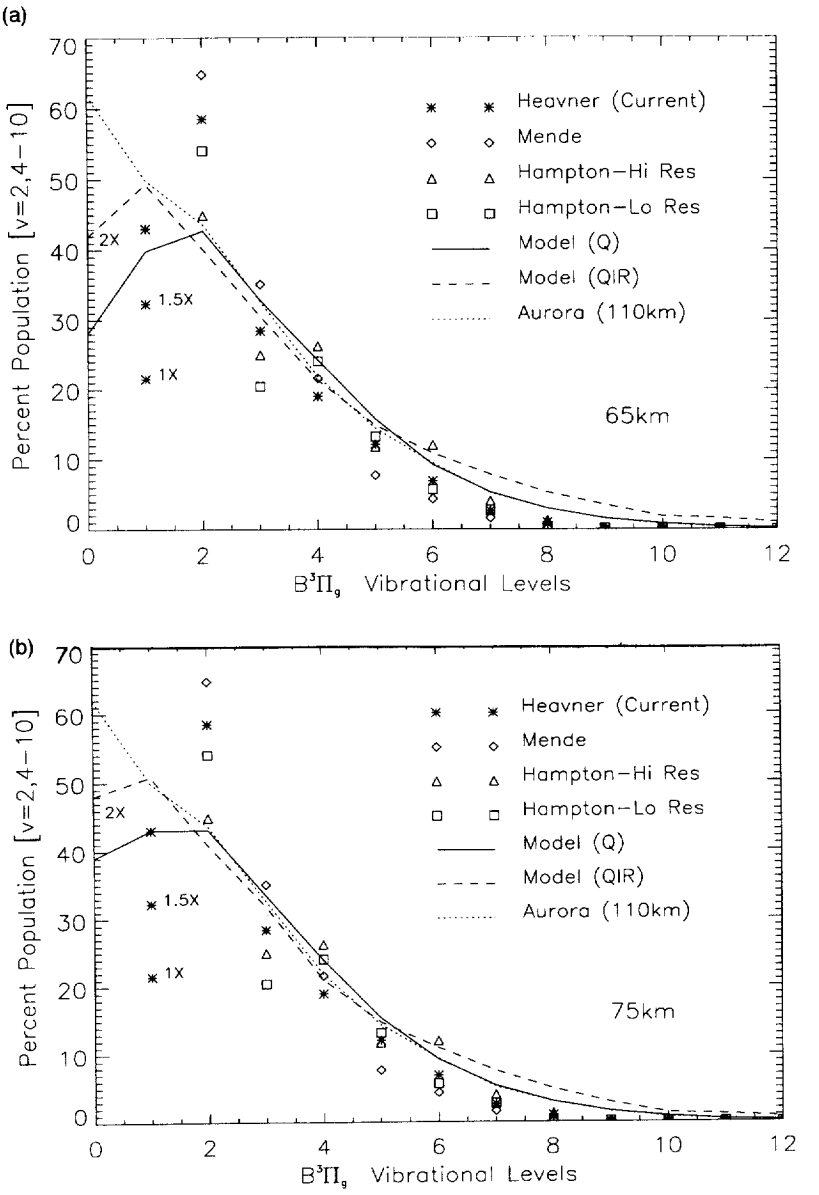

Fig. 11. Relative vibrational populations comparing quenching only (Q) and (b) quenching, ICT, vibrational redistribution (QIR) at (a) 65 km and (b) 75 km, with various measured vibrational distributions. The names refer to the conventions of Green et al. (1996) except for 'Heavner' (Heavner et al., 1996).

occurring in the shorter wavelength visible and near-UV spectral ranges (3000–5000 Å). This spectral region contains numerous N_2 and N_2^+ emission features, primarily the Vegard-Kaplan (VK, $A^3\Sigma_u^+ \rightarrow X^1\Sigma_g^+$), and Second Positive Group of N_2 and the First Negative Group (1NG, $B^2\Sigma_u^+ \rightarrow X^2\Sigma_g^+$) of N_2^+ (Vallance Jones, 1974; Cleary et al., 1995; Broadfoot et al., 1997). The current model does not contain N_2^+ species, and so we initially focus our discussion on the N_2 emissions.

In order to compare the effect of attenuation on a set of emission features in the 3000–5000 Å spectral range, we have chosen two observing conditions. First, an observation altitude of 5 km and a 500 km path length, and second, a 10 km observation altitude and a 100 km path length, both observing emissions from 65 km altitude. Model time profiles of emission associated with three spectral features are shown in Fig. 12. The features are the 1PG (2, 0), 2PG (0, 3), and VK (1, 10) vibrational

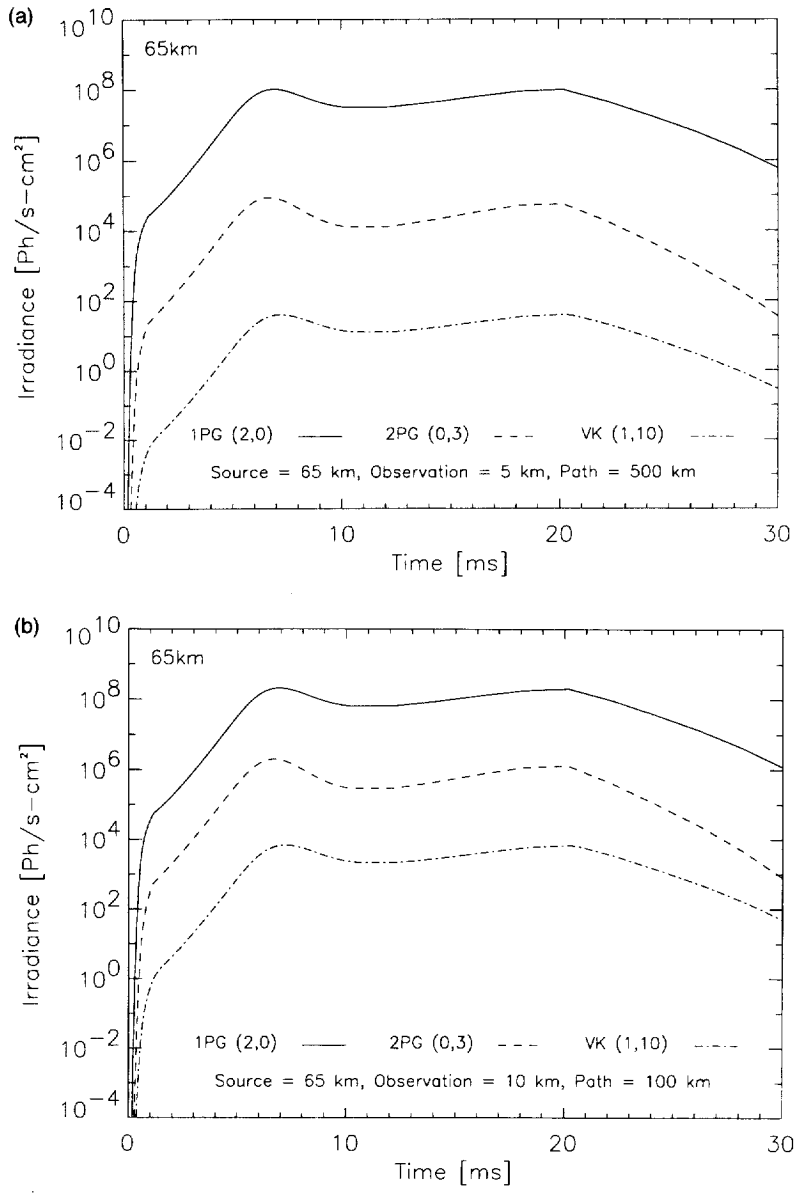

Fig. 12. Predicted temporal variation of emission for 1PG (2, 0), 2PG (0, 3), VK (1, 10) bands (a) from altitudes of 65 km to 5 km, along a 500 km path; and (b) from altitudes of 65 km to 10 km, along a 100 km path.

bands. The band origins, transition probabilities, and predicted atmospheric transmission for the above two cases are listed in Table 3. A comparison of Fig. 12a and b shows the increase in the observed intensity of all features by factors of 2, 23, 170 for the 1PG, 2PG, VK bands, respectively, when the observation altitude is increased from 5 to 10 km and the path length is decreased from 500 to 100 km. Further improvement can be realized by increasing the observation altitude from 10 km (normal aircraft) to 20 km (high altitude aircraft). Attenuation by aircraft windows has not been included, but this effect could be minimized by use of quartz viewing ports. The choice of 2PG and VK bands was based on their spectral position so that well-chosen passband filters would allow them to be observed without overlap by nearby bands (Vallance Jones, 1974, Broadfoot, 1996).

There are other emission features associated with the measurement of sprites which would benefit from measurements at higher altitudes and shorter path lengths. This involves the measurement of the lower levels of the $N_2(B)$ and $N_2^+(A)$ states. The N_2 1PG (0,0) band ($N_2(B, v = 0)$) emits at approximately 10,500 Å while the

Table 3
Transition parameters for N_2 emissions

Band	Origin (Å)	Transition Probability (1/sec)	Transmission		Ratio
			5 km–500 km	10 km–100 km	
1PG (2, 0)	7732	3.96e4	4.63e-1	9.42e-1	2
2PG (0, 3)	4058	1.10e6	3.27e-2	7.48e-1	23
VK (1, 10)	3427	9.87e-2	3.59e-3	6.16e-1	170

Transition parameters for N_2 emissions used in Fig. 12. The distances under 'Transmission' are the observing altitude and path length through the atmosphere, respectively.

N_2^+ (0, 0) and (1, 0) Meinel bands (N_2^+ (A, $v = 0, 1$)) emit at approximately 11,100 and 9200 Å. The 1PG (0, 0) occurs in a region between water absorption features, while the two N_2^+ (A) features would be strongly absorbed unless the path length were kept short and the observing altitude were kept high (≥ 10 km; see Fig. 1). Observation of these bands could be done photometrically and the population of these levels would provide important additional information about the electron energies present in red sprites.

Regarding the observed spectrum in Fig. 2, we discuss two significant points. The first is the possible presence of N_2^+ Meinel bands and the second is the observed N_2(B) vibrational distribution. With regard to the Meinel emission, the fit to the spectrum in Fig. 2 gives us portions of the relative populations of the N_2(B) and N_2^+(A) states, and these are presented in Table 4 (see Fig. 2b). Also in Table 4 are the N_2(B) and N_2^+(A) vibrational distributions measured during an ~IBC2+aurora observed by Vallance Jones and Gattinger (1978). As mentioned above, low intensity and experimental uncertainties make the present relative populations of the N_2(B) and N_2^+(A) states preliminary and are best considered upper bounds for the N_2^+(A) population in this spectrum. However, it is worthwhile examining estimates of the average electron energies required to produce the observed ratio of N_2^+ (A) to N_2(B) populations in levels 2 and 3. These estimates were made using a simplified steady-state model involving N_2(C), N_2(B) and N_2^+(A) excited by Boltzmann and quasi-electrostatic electron distributions, which includes both quenching of N_2(B) (Morrill and Benesch, 1996) and N_2^+(A) (Piper et al., 1985), as well as radiative cascade (Gilmore et al., 1992). The results for 2 eV show the N_2^+ (A)/N_2(B) ratio to be on the order of 10^{-3} and 10^{-5} for these two types of distributions, respectively.

Table 4
N_2(B) and N_2^+(A) vibrational distributions—aurora vs sprite

v	Aurora (IBC II+)		Red sprite	
	N_2(B)	N_2^+(A)	N_2(B)	N_2^+(A)
0	2.80	5.75	—	—
1	2.04	5.07	1.13	—
2	2.37	2.88	3.08	0.83
3	1.46	1.45	1.50	0.35
4	1.00	0.52	1.00	—
5	0.58	0.17	0.64	—
6	—	—	0.36	—
7	—	—	0.14	—
$\Sigma_{v=2\text{-}3}$	3.83	4.33	4.58	1.18
$N_2^+(A)/N_2(B)_{v=2\text{-}3}$	1.13		0.26	

N_2 (B) and N_2^+(A) vibrational distributions in the aurora (Vallance Jones and Gattinger, 1978) and in a red sprite (see Fig. 2).

In order to achieve a ratio of ~0.26 for the N_2^+(A, $v = 2$–3)/N_2(B, $v = 2$–3) ratio (see Table 4), average energies in the Boltzmann and quasi-electrostatic electron distributions in excess of 10 eV were required. However, Bell et al. (1995) predict volume emission rates for 1PG and Meinel excited by runaway electrons. From the ratio of the volume emission rates at 55 km ((5.7e3 ph/cc-s)/(1.6e6 ph/cc-s)) and the average radiative lifetimes (14.3e-6s/5.9e-6s), the predicted N_2^+(A) and N_2(B) populations have a ratio of ~0.086. This ratio is scaled up by factor of 1.38 in accordance with the recent branching ratio for the N_2^+(A) state (0.54) (Van Zyl and Pendleton, 1995) rather than the value (0.39) used by Bell et al. (1995). Further, to compare to the N_2^+(A)/N_2(B) ratio in Table 4, the fraction of the population in levels 2 and 3 of these two states is accounted for with a scaling factor of 1.1 (i.e. the fraction of the total population in levels 2 and 3 is roughly the same for both states, ~33%). This yields a ratio of N_2^+(A, $v = 2$–3)/N_2(B, $v = 2$–3) ~ 0.13 which is 50% of the observed ratio. Given the uncertainties in the observed ratio and the lack of an obvious explanation for the presence of the Meinel band by either the Boltzmann or quasi-electrostatic electron distributions, production of the observed spectrum—at least in part—by runaway electrons appears to be a reasonable possibility.

The above results have assumed that quenching represents a loss of population from the N_2^+(A) state based

on quenching rates reported by Vallance Jones (1974) which are similar to the values measured by Piper et al. (1985). However, Katayama et al. (1980) and Katayama (1984) have shown collisional energy transfer, similar to that discussed above (ICT), to occur rapidly between the $N_2^+(A)$ and $N_2^+(X)$ states. This type of process tends to increase the apparent lifetime of an emitting state when it is collisionally coupled to a state with a longer lifetime, as in this case. Consequently, the results by Bell et al. (1995) would underestimate the $N_2^+(A)$ state population. An increase in this population would tend to further support the above analysis of the Meinel emission.

The strongest observed spectral features are the 1PG bands. The results of Green et al. (1996) show the $N_2(B)$ vibrational distributions associated with a number of sprite spectra (Fig. 11), and indicate an average electron energy on the order of 1 eV. This is significantly lower than the auroral case (see Table 4) where, for example, the electron energy distribution in an IBC2+aurora is expected to have an average energy on the order of ~3–5 eV (Cartwright, 1978; Fig. 2). We have reached similar conclusions to those of Green et al. (1996) regarding the magnitude of electron energies in sprites based on the model $N_2(B)$ vibrational distribution shown in Fig. 11a produced by electrons with an average energy of 1–2 eV (Fig. 6). As shown in Fig. 11, the observed vibrational distributions peak at $v = 2$, unlike the auroral distribution that peak at $v = 0$. Although the population for $v = 1$ from the current spectral fit appears low, an increase in the observed intensity of the 1PG (1, 0) band at 8900 Å on the order of a factor of 2.5–3 would be required to have the observed distribution peak at $v = 1$. We are currently re-examining the intensity calibration near 9000 Å which could effect the corrected intensity of the $\Delta v = 1$ sequence and so the populations of $v = 1$ of the $N_2(B)$ state.

As mentioned above, we are currently analyzing additional sprite spectra taken with higher resolution and better red sensitivity (Bucsela et al., 1998) that yield a preliminary estimate of the $v = 1$ population at about twice the currently determined value. However, it is not necessarily the case that the summed spectrum of different regions of sprites will be identical, or nearly so, given the variability and spatial structure of sprites. Nonetheless, the persistence of the $v = 2$ enhancement observed by numerous groups (see Fig. 11) is an indication of a predominant process occurring during the 17–33 ms period of the video spectral data analyzed thus far.

Finally, an additional mechanism that is known to produce 1PG emission but which has not been included in our model is energy pooling involving the $N_2(A)$ state (Piper, 1988a, b; 1989). Here we refer to both $N_2(A)+N_2(A)$ and $N_2(A)+N_2(X, v > \sim 5)$. Since the predicted $N_2(A)$ density only reaches values on the order of 10^5 molecules/cm^3, the $N_2(A)+N_2(A)$ process is not likely to produce significant 1PG emission. However, since the vibrational excitation is ~100–1000 times larger than electronic excitation (Figs 7 and 8), there is a possibility that the process involving $N_2(A)+N_2(X, v > \sim 5)$ could contribute to the 1PG emission. However, this process leads to $N_2(B)$ vibrational distributions that are strongly peaked at the lower levels, unlike the observed distribution in Fig. 11. The spectral observations used in this paper represent data taken with TV field rate (17 ms resolution), so that portions of the observations could contain a portion due to an 'afterglow' which may have a significant effect on the observed spectrum. Higher time resolution data can be extracted from the spectrograph and the afterglow process can be modeled with further effort. Given the differences between the observed distribution and those produced by the model, further modelling and analysis of existing spectral data are warranted to determine the spatial and temporal variation of N_2 excited state vibrational distributions and the processes which produce them.

8. Conclusion

We have presented the results of a quasi-electrostatic heating model, combined with a time-dependent vibrational level populations model, in order to examine the temporal behavior of N_2 excited state populations in red sprites. In order to compare the model results with spectral observations, we have analyzed a recent sprite spectrum measured from the Wyoming Infrared Observatory (WIRO) on Jelm Mountain (Heavner et al., 1996, Bucsela et al., 1998) and have included the recent spectral analysis made by Green et al. (1996). The spectral analysis incorporates atmospheric attenuation models (e.g. MOSART), and we have discussed the effect of atmospheric attenuation on various N_2 emissions (1PG, 2PG, and VK). The effect of collisional processes other than simple quenching has also been presented and this represents a potential source of additional 1PG emission intensity.

The current spectral analysis indicates the possible presence of N_2^+ Meinel emission in addition to the N_2 1PG. However, due to the low observed intensity and experimental uncertainties the relative population of the $N_2(B^3\Pi_g)$ and $N_2^+(A^2\Pi_u)$ states should be considered as being preliminary. The current analysis yields a vibrational distribution of the $N_2(B^3\Pi_g)$ that requires an average electron energy of only 1–2 eV. Model results show that the populations of the lower levels of the $N_2(B^3\Pi_g)$ increase with increases in the electron energy. If the presence of the N_2^+ Meinel emission is confirmed in other sprite spectra this may imply the presence of runaway electrons or enhancements in the electron energy distribution. However, further spectral and photometric observations will be required at both longer and shorter wavelengths in order to improve our under-

standing of the details of the electron energy distributions which occur in sprites.

Acknowledgements

The computer time was supported by the Solar Physics Branch and X-Ray Astronomy Branch in the Space Science Division of the Naval Research Laboratory and STAR Laboratory of Stanford University. The atmospheric transmission calculations were performed using the MOSART model as implemented in the SSGM (Synthetic Scene Generation Model) at the Space Science Division of the Naval Research Laboratory. E. J. Bucsela was supported by an ASEE Postdoctoral Fellowship. J. S. Morrill was supported in part by the Edison Memorial graduate training program at the Naval Research Laboratory; V. P. Pasko was supported by an NSF Postdoctoral Fellowship under NSF grant ATM-9522816 to Stanford University; and D. R. Moudry, M. J. Heavner, D. D. Sentman, and E. M. Wescott were supported by NASA grant NAG5-5019. The authors would like to thank B. D. Green for providing the $B^3\Pi_g$ vibrational distributions, G. R. Swenson for numerous interesting conversations on red sprites, and U. S. Inan, T. F. Bell, and S. G. Queen for their critical review of the manuscript.

References

Armstrong, R.A., Shorter, J.A., Taylor, M.J., Suszcynsky, D.M., Lyons, W.A., Leong, L.S., 1998. Photometric measurements in the SPRITES '95 & '96 campaigns, nitrogen second positive (399.8 mn) and first negative (427.8 nm) emission. J. Atmos. Sol. Terr. Phys. 60, 787–799.

Bell, T.F., Pasko, V.P., Inan, U.S., 1995. Runaway electrons as a source of red sprites in the mesosphere. Geophys. Res. Lett. 22, 2127–2130.

Benesch, W., 1981. Mechanism for the auroral red lower border. J. Geophys. Res. 86, 9065–9072.

Benesch, W., 1983. Intersystem collisional transfer of excitation in low altitude aurora. J. Chem. Phys. 78, 2978–2983.

Benesch, W., Fraedrich, D. 1984. The role of intersystem collisional transfer of excitation in the determination of N_2 vibronic level populations. Application to $B'^3\Sigma_u^- - B^3\Pi_g$ band intensity measurements. J. Chem. Phys. 81, 5367–5374.

Berk, A., Bernstein, L.S., Robertson, D.C., 1989. MODTRAN: A Moderate Spectral Resolution Model for LOWTRAN7, Phillips Laboratory Report No. GL-TR-89-0122.

Broadfoot, A.L., Hatfield, D.B., Anderson, E.R., Stone, T.C., Sandel, B.R., Murad, E., Hecht, D.J., Pike, C.P., Viereck, R.A., Gardner, J.A., 1997. The N_2 triplet band systems and atomic oxygen in the dayglow. J. Geophys. Res., 102, 11567–11584.

Bucsela, E.J., Sharp, W.E., 1997. NI 8680 and 8629 Å multiplets in the dayglow. J. Geophys. Res. 102, 2457–2466.

Bucsela, E.J., Heavner, M.J., Morrill, J.S., Pasko, V.P., Berg, S.L., Moudry, D.R., Benesch, W.M., Wescott, E.M., Sentman, D.D., 1998. The visible and near-IR spectroscopy of red sprites. Geophys. Res. Lett. in preparation.

Caledonia, G.E., Center, R.E. 1971. Vibrational distribution functions in anharmonic oscillators. J. Chem. Phys. 55, 552–561.

Carragher, B.A., Morrill, J., Benesch, W. 1991a. Gas-phase molecular energy transfer studies with time-resolved spectroscopy. J. Opt. Soc. Am., B. 8, 123–128.

Carragher, B.A., Morrill, J., Benesch, W. 1991b. Gas-phase molecular energy transfer studies with time-resolved spectroscopy: errata. J. Opt. Soc. Am., B. 8,

Cartwright, D.C., 1978. Vibrational populations of the excited states of N_2 under auroral conditions. J. Geophys. Res. 83, 517–531.

Cleary, D.D., Gnanalingam, S., McCoy, R.P., Dymond, K.F., Eparvier, F.G., 1995. The middle ultraviolet dayglow spectrum. J. Geophys. Res. 100, 9729–9739.

Cornette, W.M., 1990. Atmospheric Propagation and Radiative Transfer (APART) Computer Code (Version 7.00), R-062-90, Photon Research Associates, Inc.

Cornette, W.M., Acharya, P.K., Anderson, G.P., 1994. Using the MOSART code for atmospheric correction. IEEE Conf. Proc. Int. Geosci., and Rem. Sens. Sympos. 1, 215–219.

Eastes, R.W., Dentamaro, A.V., 1996. Collision-induced transitions between the $a^1\Pi_g$, $a'^1\Sigma_u$, and $w^1\Delta_u$ states of N_2: Can they effect auroral N_2 Lyman-Birge-Hopfield band emission. J. Geophys. Res. 101, 26931–26940.

Fishman, G.J., Bhat, P.N., Mallozzi, R., Horack, J.M., Koshut, T., Kouveliotou, C., Pendleton, G.N., Meegan, C.A., Wilson, R.B., Paciesas, W.S., Goodman, S.J., Christian, H.J., 1994. Discovery of intense gamma-ray flashes of atmospheric origin. Science 264, 1313–1316.

Fraser, M.E., Rawlins, W.T., Miller, S.M., 1988. Infrared (2–8 μm) fluorescence of the $W^3\Delta_u \rightarrow B^3\Pi_g$ and $w^1\Delta_u \rightarrow a^1\Pi_g$ systems of nitrogen. J. Chem. Phys. 88, 538–544.

Fukunishi, H., Takahashi, Y., Kubota, M., Sakanoi, K., Inan, U.S., Lyons, W.A., 1996a. Lightning-induced transient luminous events in the lower ionosphere. Geophys. Res. Lett. 23, 215–216.

Fukunishi, H., Takahashi, Y., Fujito, M., Watanabe, Y., Sakanoi, S., 1996b. Fast imaging of elves and sprites using a framing/streak camera and a multi-anodo array photometer. EOS Trans. AGU, 77, F60, Fall Meet. Suppl., A71B-2.

Green, B.D., Fraser, M.E., Rawlins, W.T., Jeong, L., Blumberg, W.A.M., Mende, S.B., Swenson, G.R., Hampton, D.L., Wescott, E.M., Sentman, D.D., 1996. Molecular excitation in sprites. Geophys. Res. Lett. 23, 2161–2164.

Gurevich, A.V., Milikh, G.M., Roussel-Dupre, R.A., 1992. Runaway electron mechanism of air breakdown and preconditioning during a thunderstorm. Phys. Lett. A 165, 463.

Gurevich, A.V., Milikh, G.M., Roussel-Dupre, R.A., 1994. Non-uniform runaway air breakdown. Phys. Lett. A 187, 197.

Gilmore, F.R., Laher, R.R., Espy, P.J., 1992: Franck-Condon factors, r-centroids, electronic transition moments, and Einstein coefficients for many nitrogen and oxygen systems. J. Phys. Chem. Ref. Data 21, 1005–1107.

Hampton, D.L., Heavner, M.J., Wescott, E.M., Sentman, D.D. 1996. Optical spectral characteristics of sprites. Geophys. Res. Lett. 23, 89–92.

Heavner, M.J., Moudry, D.R., Sentman, D. D., Wescott, E.M.,

Desroschers, J.T., 1996. Spectral observations of sprites (abstract). Eos Trans. AGU, 77 (46) Fall Meet. Suppl., 60.

Hedin, A.E., 1991. Extension of the MSIS thermosphere model into the middle and lower atmosphere. J. Geophys. Res. 96, 1159.

Huber, K.P., Herzberg, G., 1979. Molecular Spectra and Molecular Structure: IV Constants of Diatomic Molecules. Van Nostrand Reinhold, New York.

Inan, U.S., Reising, S.C., Fishman, G.J., Horack, J.M., 1996. On the association of terrestrial gamma-ray bursts with lightning and implications for sprites. Geophys. Res. Lett. 23, 1017–1020.

Katayama, D.H., 1984. Collision induced electronic energy transfer between the $A^2\Pi_u$ ($v = 4$) and $X^2\Sigma_g^+$ ($v = 8$) rotational manifolds of N_2^+. J. Chem. Phys. 81, 3495–3494.

Katayama, D.H., Miller, T.A., Bondybey, V.E., 1980. Collisional deactivation of selectively excited N_2^+. J. Chem. Phys. 72, 5469–5475.

Laher, R.R., Gilmore, F.R., 1991. Improved fits for the vibrational and rotational constants of many states of nitrogen and oxygen. J. Phys. Chem. Res. Data 20, 685–712.

Lehtinen, N.G., Walt, M., Inan, U.S., Bell, T.F., Pasko, V.P., 1996: γ-ray emission produced by a relativistic beam of runaway electrons accelerated by quasi-electrostatic thundercloud fields. Geophys. Res. Lett. 23, 2645–2648.

Lehtinen, N.G., Bell, T.F., Pasko, V.P., Inan, U.S., 1997. A two-dimensional model of runaway electron beams driven by quasi-electrostatic thundercloud fields. Geophys. Res. Lett. 24, 2639–2642.

McCarthy, M.P., Parks, G.K., 1992. On the modulation of X ray fluxes in thunderstorms. J. Geophys. Res. 97, 5857–5864.

Mende, S.B., Rairden, R.L., Swenson, G.R., Lyons, W.A., 1995. Sprite spectra: N_2 1PG band identification. Geophys. Res. Lett. 22, 2633–2636.

Milikh, G.M., Papadopoulos, K., Chang, C.L., 1995. On the physics of high altitude lightning. Geophys. Res. Lett. 22, 85–8.

Milikh, G.M., Valdivia, J.A., Papadopoulos, K., 1997. Model of red sprite optical spectra. Geophys. Res. Lett. 24, 833–836.

Morrill, J.S., 1986. The effect of collisions and plasma preconditioning on the vibrational level population of molecular nitrogen. Thesis, Univ. of Md., College Park.

Morrill, J., et al., Carragher, B.A., Benesch, W., 1988. Population development of auroral molecular nitrogen species in a pulsed discharge. J. Geophys. Res. 93, 963–977.

Morrill, J., Benesch, W., 1990. Plasma preconditioning and the role of elevated vibrational temperature in production of excited N_2 vibrational distributions. J. Geophys. Res. 95, 7711–7724.

Morrill, J.S., Benesch, W.M., Widing, K.G., 1991. Electron temperatures in a pulse electric discharge and the associated N_2 electron excitation rate coefficients. J. Chem. Phys. 94, 262–269.

Morrill, J.S., Benesch, W.M., 1994. The role of $N_2(A'^5\Sigma_g^+)$ in the enhancement of N_2 $B^3\Pi_g$ ($v = 10$) populations in the afterglow. J. Chem. Phys. 101, 6529–6537.

Morrill, J.S., Benesch, W.M., 1996. Auroral N_2 emissions and the effect of collisional processes on N_2 triplet state vibrational populations. J. Geophys. Res. 101, 261–274.

Papadopoulos, K., Milikh, G., Gurevich, A., Drobot, A., Shanny, R., 1993. Ionization rates for atmospheric and ionospheric breakdown. J. Geophys. Res. 98, 17593–17596.

Pasko, V.P., Inan, U.S., Taranenko, Y.N., Bell, T.F., 1995. Heating, ionization and upward discharges in the mesosphere due to intense quasi-electrostatic thundercloud fields. Geophys. Res. Lett. 22, 365–368.

Pasko, V.P., 1996. Dynamic coupling of quasi-electrostatic thundercloud fields to the mesosphere and lower ionosphere: sprites and jets, Ph.D. dissertation, Stanford. University of California.

Pasko, V.P., Inan, U.S., Bell, T.F., 1996. Sprites as luminous columns of ionization produced by quasi-electrostatic thundercloud fields. Geophys. Res. Lett. 23, 649–652.

Pasko, V.P., Inan, U.S., Bell, T.F., Taranenko, Y.N., 1997a. Sprites produced by quasi-electrostatic heating and ionization in the lower ionosphere. J. Geophys. Res., 102, 4529.

Pasko, V.P., Inan, U.S., Bell, T.F., 1997b. Gravity waves above mesoscale thunderstorms and small scale structure of sprites, (abstract). Eos Trans. AGU, Spring meet. Suppl.

Pavlov, A.V., Buonsanto, M.J. 1996. Using steady state vibrational temperatures to model effects of N_2^* on calculations of electron densities. J. Goephys. Res. 101, 26,941–26,945.

Phelps, A.V., 1987. Excitation and ionization coefficients. Gaseous Dielectric 5, 1–9.

Piper, L.G., 1988a. State-to-state $N_2(A^3\Sigma_u^+)$ energy pooling reactions. I. The formation and quenching of $N_2(C)$ $^3\Pi_u$) and Herman infrared system. J. Chem. Phys. 88, 231–239.

Piper, L.G., 1988b. State-to-state $N_2(A^3\Sigma_u^+)$ energy pooling reactions. II. The formation and quenching of $N_2(B^3\Pi_g, v = 1$–$12)$, J. Chem. Phys. 88, 6911–6921.

Piper, L.G., 1989. The excitation of $N_2(B^3\Pi_g, v = 1$–$12)$ in the reaction between $N_2(A^3\Sigma_u^+)$ and $N_2(X, v \geqslant 5)$, J. Chem. Phys. 91, 864–873.

Piper, L.G., 1993. Reevaluation of the transition-moment function and Einstein coefficients for the $N_2(A^3\Sigma_u^+ - X^1\Sigma_g^+)$ transition. J. Chem. Phys. 99, 3174–3181.

Piper, L.G., Holtzclaw, K.W., Green, B.D., 1989. Experimental determination of the Einstein coefficients for the $N_2(B-A)$ transition. J. Chem. Phys. 90, 5337–5345.

Richard, A., de Souza, A.R., 1994. Active species in N_2 flowing post-discharges. J. Phys. III France 4, 2593–2600.

Roussel-Dupre, R.A., Gurevich, A.V., Tunnell, T., Milikh, G.M., 1994. Kinetic theory of runaway air breakdown. Phys. Rev. E 49, 2257.

Roussel-Dupre, R.A., Gurevich, A.V., 1996. On runaway breakdown and upward propagating discharges. J. Geophys. Res. 101, 2297.

Rowland, H.L., Fernsler, R.F., Huba, J.D., Bernhardt, P.A., 1996. Lightning driven EMP on the upper atmosphere. Geophys. Res. Lett. 22, 361.

Rowland, H.L., Fernsler, R.F., Bernhardt, P.A., 1996.Breakdown of the neutral atmosphere in the D-region due to lightning driven electromagnetic pulses. J. Geophys. Res. 101, 7935–7945.

Rowland, H.L., 1998. Theories and simulations of elves, sprites, and blue jets. J. Amos. Solar Terr. Phys. 60, 831–844.

Sentman, D.D., Wescott, E.M., Osborne, D.L., Hampton, D.L., Heavner, M.J., 1995. Preliminary results from the Sprites 94 campaign: Red sprites. Geophys. Res. Lett. 22,1205–1208.

Sentman, D.D., Wescott, E.M., Heavner, M.J., Moudry, D.R., 1996: Observations of sprite beads and balls. EOS Trans. AGU, 77, F61, Fall Meet. Suppl., A71B-7.

Stanley, M., Krehbiel, P., Rison, W., Moore, C., Brook, M., Vaughan, O.H., 1996. Observations of sprites and jets from Langmuir laboratory, New Mexico. EOS Trans. AGU, 77, F69, Fall Meet. Suppl., A11A-7.

Taranenko, Y.N., Inan, U.S., Bell, T.F., 1993a. The interaction with the lower ionosphere of electromagnetic pulses from lightning: heating, attachment, and ionization. Geophys. Res. Lett. 20, 1539–1542.

Taranenko, Y.N., Inan, U.S., Bell, T.F., 1993b. The interaction with the lower ionosphere of electromagnetic pulses from lightning: excitation of optical emissions. Geophys. Res. Lett. 20, 2675–2678.

Taranenko, Y.N., Roussel-Dupre, R.A., 1996. High altitude discharges and gamma-ray flashes: a manifestation of runaway air breakdown. Geophys. Res. Lett. 23, 571–574.

Taylor, M.J., Clark, S., 1996. High resolution CCD and video imaging of sprites and elves in the N_2 first positive band emission. EOS Trans. AGU, 77, F60, Fall Meet. Suppl., A71B-4.

Torr, D.G., Torr, M.R., 1982. The role of metastable species in the thermosphere, Rev. Geophys. Space Phys., 20, 91–144.

Trajmar, S., Register, D.F., Chutjian, A., 1983. Electron scattering by molecules by molecules, II, Experimental methods and data. Phys. Rep., 97, 219–356.

Vallance Jones, A., 1974. Aurora, Geophysics and Astrophysics Monographs, D. Reidel, Hingham, Mass, U.S.A.

Vallance Jones, A., Gattinger, R.L., 1974. Quantitative spectroscopy of the aurora, IV; the spectrum of medium intensity aurora between 8800 Å and 11400 Å. Can. J. Phys. 54, 2128–2133.

Vallance Jones, A., Gattinger, R.L., 1978, Vibrational development and quenching effects in the $N_2(B^3\Pi_g - A^3\Sigma_u^+)$ and $N_2^+(A^2\Pi_u - X^2\Sigma_g^+)$ system in aurora. J. Geophys. Res. 83, 3255–3261.

Van Zyl, B., Pendleton, Jr., W., 1995. $N_2^+(X)$, $N_2^-(A)$, and $N_2^+(B)$ production in $e^- + N_2$ collisions. J. Geophys. Res. 100, 23,755–23,762.

Wescott, E.M., Sentman, D.D., Heavner, M.J., Moudry, D.R., 1996. Blue jets, lightning and large hail. EOS Trans. AGU, 77, F67, Fall Meet. Suppl., A72C-3.

Wilcoxen, B., Heckathorn, H., 1996. Synthetic Scene Generation Model (SSGM R7.0), in Targets and Backgrounds: Characterization and Representation II. Proceedings of the International Society for Optical Engineering 2742, 57–68.

Zubek, M., 1994: Excitation of the $C^3\Pi_u$ state of N_2 by electron impact in the near-threshold region. J. Phys. B: At. Mol. Opt. Phys. 27, 573–581.

Zubek, M., King, G.C., 1994. Differential cross sections for electron impact excitation of the $C^3\Pi_u$, $E^3\Sigma_g^+$, and $a'^1\Sigma_u^-$ states of N_2. J. Phys. B: AT. Mol. Opt. Phys. 27, 2613–2624.